

Design and optimization of nano-antenna for thermal ablation of liver cancer cells

Mohammad Javad Rabienejhad[1], Azardokht Mazaheri[2,†], and Mahdi Davoudi-Darareh[3]

Citation: Chin. Phys. B, 2021, 30 (**4**): 048401. DOI: 10.1088/1674-1056/abd38e
Journal homepage: http://cpb.iphy.ac.cn; http://iopscience.iop.org/cpb

What follows is a list of articles you may be interested in

Stretchable electromagnetic interference shielding and antenna for wireless strain sensing by anisotropic micron-steel-wire based conductive elastomers

Xiaoyu Hu(胡晓宇), Linlin Mou(牟琳琳), and Zunfeng Liu(刘遵峰)
Chin. Phys. B, 2021, 30 (**1**): 018401. DOI: 10.1088/1674-1056/abc2b3

Dual-polarized lens antenna based on multimode metasurfaces

Hao-Fang Wang(王浩放), Zheng-Bin Wang(王正斌), Yong Cheng(程勇), Ye-Rong Zhang(张业荣)
Chin. Phys. B, 2018, 27 (**11**): 118401. DOI: 10.1088/1674-1056/27/11/118401

Correction of failure in antenna array using matrix pencil technique

S U Khan, M K A Rahim
Chin. Phys. B, 2017, 26 (**6**): 068401. DOI: 10.1088/1674-1056/26/6/068401

Metallic spherical anechoic chamber for antenna pattern measurement

Ali Farahbakhsh, Mohammad Khalaj-Amirhosseini
Chin. Phys. B, 2016, 25 (**8**): 088401. DOI: 10.1088/1674-1056/25/8/088401

An ultra-wideband pattern reconfigurable antenna based on graphene coating

YanNan Jiang(姜彦南), Rui Yuan(袁锐), Xi Gao(高喜), Jiao Wang(王娇), SiMin Li(李思敏), Yi-Yu Lin(林诒玉)
Chin. Phys. B, 2016, 25 (**11**): 118402. DOI: 10.1088/1674-1056/25/11/118402

Design and optimization of nano-antenna for thermal ablation of liver cancer cells

Mohammad Javad Rabienejhad[1], Azardokht Mazaheri[2,†], and Mahdi Davoudi-Darareh[3]

[1] *Optics and Laser Science and Technology Research Center, Malek Ashtar University of Technology, Shahinshahr, Iran*
[2] *Department of Physics, University of Isfahan, Iran*
[3] *Faculty of Science, Malek Ashtar University of Technology, Shahinshahr, Iran*

(Received 22 September 2020; revised manuscript received 7 November 2020; accepted manuscript online 15 December 2020)

One method of cancer therapy is to utilize nano-antenna for thermal ablation. In this method, the electromagnetic waves emitted from the nano-antenna are absorbed by the tissue and lead to heating of cancer cells. If temperature of cancer cells reaches a threshold, they will begin to die. For this purpose, an L-shaped frame nano-antenna (LSFNA) is designed to introduce into the biological tissue. Thus, the radiation characteristics of the LSFNA such as near and far-field intensities, directivity, and sensitivity to its gap width are studied to the optimization of the nano-antenna. The bio-heat and Maxwell equations are solved using the finite element method. To prevent damage to healthy tissues in this method, the antenna radiation must be completely controlled and performed carefully. Thus, penetration depth, special absorption rate, temperature distribution, and the fraction of tissue necrosis are analyzed in the biological tissue. That is why the design and optimization of the nano-antennas as a radiation source is important. Also, a pulsed source is used to excite the LSFNA. Furthermore, focusing and efficiency of the nano-antenna radiation on the cancer cell is tuned using an adjustable liquid crystal lens. The focus of this lens is changing under an electric field applied to its surrounding cathode.

Keywords: cancer therapy, directivity, far-field intensity, hyperthermia, liver cancer, nano-antenna, thermal-ablation, tunable liquid crystal lens

PACS: 84.40.Ba, 64.70.mf, 52.38.Mf, 87.19.xj **DOI:** 10.1088/1674-1056/abd38e

1. Introduction

Today, various methods are utilized in cancer treatment, which always face many challenges. Because in traditional surgery, it is almost impossible to destroy cancer cells without damaging adjacent normal cells.[1] Although surgery is a usual method for removing tumors, there are many cases in which surgery is not possible to remove due to the unfavorable location of the cancer cells or the presence of multiple tumors. As a result, alternative surgical methods such as chemotherapy and radiation therapy are utilizing in combination or alone.[2] However, conventional chemotherapy and radiation treatments require regular treatment duration for several weeks and using high doses of anticancer drugs or utilizing high-energy x-rays. These conditions can lead to many side effects such as redness of skin, vomiting, hair loss, and many other conditions without guaranteeing complete ablation of tumors.[2–4]

In contrast, non-surgical tumor ablation methods have developed. These methods are more accurate and faster than traditional cancer treatment methods. Also, they are painless, without the need for prolonged hospitalization, and low costs.[4,5] However, non-surgical ablation treatments have their challenges, such as achieving a balance between radiation and accurate targeting of cancer cells and minimizing damage to healthy cells in the vicinity of a tumor. Nanotechnology has provided facilities for direct entry into tumors, ablation of cancer cells, and overcoming these challenges by increasing treatment efficiency.[6–9] One of the nanotechnology devices in the field of cancer treatment is the nano-antenna. The nano-antennas[10–12] are the metal nanostructures equivalent to radio-frequency and microwave antennas.[13–15] The nano-antennas can enhance, confine, transmit, and receive light fields in nanoscale dimensions.[16–20] The most widely used nano-antenna fabrication technique is electron beam lithography (EBL). This method has high flexibility and accuracy in constructing complex nanoscale structures.[21] However, using this method in the mass production of the nano-antenna is not affordable. Also, due to the production process in this method, the available height of nanostructures is limited to about 50 nm. Therefore, EBL cannot be easily used to produce nano-antennas with high thickness characteristics.[22] Another common lithography technique for nano-antenna fabrication is the focused ion beam (FIB) milling, which is ideal for the production of slot nano-antenna in metal films. Similarly to EBL, FIB has significant disadvantages, including very low throughput (typically 10 to 13 m^2/s with a high resolution of 30% milling coefficient).[23,24] However, soft lithography can overcome these limitations and various disadvantages of EBL and FIB.[25] Also, it can create arrays with a large area of the nano-antennas with high accuracy. Soft lithography consists of a set of patterning techniques that use elastomeric masks (e.g., polydimethylsiloxane (PDMS)) to construct the nano-antenna arrays.[25–27] The soft-nanolithographic process can be divided into four main steps for large-scale fabrication of

†Corresponding author. E-mail: dokht2001@yahoo.com

© 2021 Chinese Physical Society and IOP Publishing Ltd

the nano-antenna arrays: (1) making a master with nanoscale properties; (2) molding the PDMS mask from the master; (3) creating a photoresist pattern; and (4) preparing and assigning a photoresist pattern to the array of the nano-antennas.[25,28–30]

Nano-antennas have significant medical applications for treatment, diagnosis, and prevention.[31–33] Depending on the nano-antenna design, it can be used as receivers or transmitters in different regions of the electromagnetic spectrum.[12,34–36] The most significant advantage of the nano-antennas over traditional surgical methods is the complete elimination of cancer cells without damaging adjacent healthy cells. Among the various medical applications of the nano-antennas are bioassay, cell imaging, tissue delivery, cancer therapy, and radiation therapy.[8,37–39] The radiation therapy process is based on the absorption of light by the tissue and its conversion into local heat. Therefore, in this treatment method, the temperature of cancer cells increased to a certain level of heat in the body, which is called hyperthermia. Increasing the temperature of the tumor kills the cancer cells.[40,41] The hyperthermia involves various methods such as thermal ablation in microwave and radio frequencies and nano-antenna and laser ablation.[42–48] Choosing the proper thermal ablation method is depending on the properties of the tumor. For example, the thermal ablation of tumors close to the surface of the skin performs by laser. However, when the tumor is positioned deeply in the body, high-frequency laser waves destroy the background tissue and water content. Therefore, it is a dangerous method for killing deep tumors.[49,50] Thus, this problem illustrates the requirement for proper methods which can be used to kill deeper cancer cells by thermal ablation. Also, another parameter that plays an important role in determining the appropriate thermal ablation method is the size of a tumor tissue. For example, if the size of the tumor is about a few tens of centimeters, the microwave antenna is needed.[51–53] In this method, if the tumor tissue is exposed to microwave radiation for one hour, and the temperature approximately rises to 52 °C, the cancer cells will be damaged.[54–56] However, the heat-generating process should be carefully monitored because a high temperature will destroy healthy tissue. Also, this method is faced to some limitations. For example, the microwave ablation method has a low performance on small tumors. There is a high risk of destroying healthy tissues using this method in small tumors. Also, this method has low radiation accuracy.[57]

One method that has higher accuracy compared to thermal ablation with microwave antennas and is less sensitive to tumor size is thermal ablation using the nano-antennas.[58,59] The simplest way to use the nano-antennas in cancer treatment is to use them as a drug delivery method.[8,32] One benefit of this method is the increased effectiveness of anticancer drugs injected into tumor tissues. In this procedure, a combination of the anticancer drugs and the nano-antennas are injecting into the tumor tissues. The tumor tissues are vascular and has many blood and lymph vessels such as veins, capillaries, and arteries. As a result, weak lymphatic secretion increases the retention of these compounds in tumor tissues. Finally, the drug reaches cancer cells by absorbing the waves emitted by the nano-antennas.[6,7,32] However, one of the main disadvantages of this method is the possibility of spreading the injected drug-nano-antennas compound throughout the body by the bloodstream. Hence, it will cause many side effects for patients or reduce the effectiveness of the treatment. Also, due to the random distribution of the injected nano-antennas into the tumor[7] and their low directivity, the accuracy of this method in killing cancer cells is low.

To overcome this challenge, the radiation characteristics of a gold simple electric dipole nano-antenna (SEDNA) such as near-field, far-field, and directivity are studied, and enhancement effects of using an L-shaped gold frame around the SEDNA are investigated. Then, an array of the L-shaped dipole nano-antenna (LSFNA) is formed to insert into a cancerous tumor of the liver tissue by a modified catheter. After the thermal ablation process, the LSFNA array will come out entirely from the body. Using the L-shaped frame (LSF) has been performed to improve the radiation characteristics of the SEDNA (such as far-field, directivity, and sensitivity to the gap width). The LSF concentrates the nano-antenna radiated energy in one direction (z-axis) and thus adjusts the radiation characteristics of the nano-antenna. Another advantage of the proposed nano-antenna is the simplicity and ease of construction using dry and wet etching methods in soft lithography, which shows the superiority of the LSFNA compared to similar nano-antennas such as bow tie and core-shell.[60,61] Since the heat should be carefully generated within the tumor, a pulsed power supply must be applied to excite the LSFNA. Therefore, in this study, the electromagnetic and bio-heat equations[42] are simultaneously solved to calculate the temperature distribution diagrams within the liver tissues. Also, the proper excitation input power of the LSFNA and the antenna radiation duration required for the thermal ablation are calculated. Thus, the optional dimensions of the LSFNA are obtained based on these calculations. The optimal geometric dimensions are obtained with the least probability of damage to healthy cells. To calculate the optimal dimensions of the LSFNA, we have also used the nano-antenna intrinsic and radiation characteristics (such as impedance, the near-field, and far-field intensities, directivity, etc). Additionally, an adjustable liquid crystal lens is placed in front of the LSFNA array to increase the radiation accuracy of the proposed antenna and reduce the risk of damage to healthy tissue. By applying an electric potential difference at the surrounding cathode of the lens, the rotation of the LCs will change. As a result, the lens focal point adjusted in this way. The electromagnetic and the thermodynamic calculations of this research performed using the finite element method.[11,61,62] The antenna proposed

in this study is similar to the antennas used for the thermal ablation of cancerous tumors at microwave frequency. However, using the proposed antenna based on the LSFNA array and a modified catheter has not been reported experimentally. As a result, the proposed antenna is a novel design in the field of using nano-antennas to treat cancer based on thermal ablation. It is worth noting that the results obtained by simulation show that some of the limitations of microwave antennas in thermal ablation and especially some of the disadvantages of using the drug-nano-antenna solution in the cancer treatment are solved with the proposed antenna.

2. Description and formulation of the problem

In numerical simulations of the electromagnetic effects on biological tissue, the calculation of penetration depth is very significant. Evaluation of penetration depth into a tissue at some particular wavelength is even more critical for thermal ablation therapy with the optical antenna. The penetration depth can be obtained by calculating the electric field distributed in the tissue. In our proposed model, it is assumed that the antenna walls are fully conductive. Also, the tissue is considered as a homogenous, linear, and isotropic environment. The wave equation is derived from the Maxwell equation

$$\nabla \times (\nabla \times \boldsymbol{E}) - \mu_{\mathrm{r}} k_{\mathrm{p}}^2 \left(\varepsilon_{\mathrm{r}} - \mathrm{j}\frac{\sigma}{\omega \varepsilon_0}\right) \boldsymbol{E} = 0, \tag{1}$$

where $\boldsymbol{E}$ is the electric field, μ_{r} the differential permeability, k_{p} the propagation constant of free space, and ε_{r} the relative permittivity. Also, ε_0 is the relative vacuum permittivity, σ denotes the electric conductivity of the biological tissue, and $\omega = 2\pi f$ is the angular frequency.[64,65]

By solving Eq. (1) for a point source in the tissue, it is possible to calculate the electric field that is radiated from the antenna into the liver tissue,[11]

$$\begin{aligned}\boldsymbol{E} = {} & \frac{J}{2\pi} \mathrm{e}^{-\mathrm{j}kr} \left(\frac{\eta}{r^2} + \frac{1}{\mathrm{j}\omega \varepsilon^* r^3}\right) \cos\theta \hat{r} \\ & + \frac{J}{4\pi} \mathrm{e}^{-\mathrm{j}kr} \left(\frac{\mathrm{j}\omega\mu}{r} + \frac{\eta}{r^2} + \frac{1}{\mathrm{j}\omega\varepsilon^* r^3}\right) \sin\theta \hat{r}.\end{aligned} \tag{2}$$

In Eq. (2), J is the source current density, κ is the complex wavenumber in liver tissue, η is the intrinsic impedance, ε^* is the complex permittivity, r is the radial distance from the point source, and θ is the angle between the observation vector and the axis along the nanoantenna length.

During the thermal ablation of the biological tissue, which is initially at the average body temperature of $T_0 =$ 37 °C, it is irradiated by an external heat source (nanoantenna). The mechanism of heat transfer in liver tissues includes a combination of their thermal conduction, blood convection and perfusion, and metabolic heat production. Here, a biological tissue of liver is studied. To finding a local thermal equilibrium (between tissue and blood), the Pence equation is widely used to model heat transfer in biological tissue.[66] This equation can be written as

$$\rho C \frac{\partial T}{\partial t} = k\nabla^2 T + \rho_{\mathrm{b}} C_{\mathrm{b}} \nu_{\mathrm{b}} (T_{\mathrm{b}} - T) + Q_{\mathrm{m}} + Q_{\mathrm{ext}}, \tag{3}$$

where ρ is the tissue density, C is the specific heat capacity of the tissue, T is the tissue temperature, k is the thermal conductivity of tissue, ρ_{b} is the blood density, C_{b} is the specific heat capacity of the blood, $\nu = \nu_0 + aT$ is the blood perfusion with the amount of $\nu_0 = 6.08 \times 10^{-3}$ s^{-1} and $a = 2.1 \times 10^{-5}$ s^{-1}°C^{-1}. Note that heat transfer in living tissues depends on blood perfusion through vascular networks.[67] The temperature difference between the tissue and the blood that flows through it causes convective heat transfer. Therefore, the blood perfusion rate is a function of temperature. Q_{m} is the heat generated by metabolism, which is negligible compared to ν_{b}. Also, $Q_{\mathrm{ext}} = \sigma|\boldsymbol{E}|^2/2 = (1/2)\,\mathrm{Re}[(\sigma - \mathrm{i}\omega\varepsilon)\boldsymbol{E}\cdot\boldsymbol{E}^*]$ is the external source which equals the heat of the resistance produced by the electromagnetic field. The relationship between the external heat source (Q_{ext}) and the specific absorption rate (SAR) is defined as follows:[68]

$$\frac{Q_{\mathrm{ext}}}{\rho} = \mathrm{SAR} = \sigma_{\mathrm{liver}}|\boldsymbol{E}|^2/2\rho. \tag{4}$$

In the simulated model, the thermal properties of the liver and tumor tissue are listed in Table 1.[54]

Table 1. The thermal properties of liver tissue used in the simulation.

Parameter	Expression	Description
$\rho_{\mathrm{liver}}(T)$	$1300 - 300W_{\mathrm{a}}(T)$	liver density
$k_{\mathrm{liver}}(T)$	$4190[0.133 + 1.36W_{\mathrm{a}}(T)]$	thermal conductivity
$C_{\mathrm{p.liver}}(T)$	$0.419[0.37 + 0.6W_{\mathrm{a}}(T)]$	specific heat capacity
ρ_{tumor}	1040 (kg/m^3)	tumor density
k_{tumor}	0.57 (W/m·°C)	thermal conductivity
$C_{\mathrm{p.tumor}}$	3960 (J/kg·K)	specific heat capacity
ν_{b}	$0, 5, 10$ (kg/m^3·s)	nominal blood perfusion rate
C_{b}	3600 (J/kg·K)	specific heat capacity of blood

Note that the temperature used in Table 1 is in units of °C. The parameter $W_{\mathrm{a}}(T)$ specifies the amount of remaining tissue water content versus temperature of the liver tissue,[68] which is defined as follows:

$$W = \begin{cases} 0.778 - 0.779\exp\left(\dfrac{T-106}{3.42}\right), & T < 103\ ^\circ\mathrm{C}, \\ -0.03924 - (T-103) + 0.454392, & 103\ ^\circ\mathrm{C} < T < 104\ ^\circ\mathrm{C}, \\ 0.778 \times \exp\left(-\dfrac{T-80}{34.37}\right), & T > 104\ ^\circ\mathrm{C}. \end{cases} \tag{5}$$

The blood flow creates a convective heat flux between the bloodflow and the tissue. This heat flux depends on the temperature difference $(T_b - T)$ in Eq. (3) and the blood flow rate. Hence, it is affected by blood perfusion.[69] Also, the boundaries of the liver tissue are assumed to be heat flux. In our purpose system, the amount of high temperature induced by the nano-antenna is less than 103 °C.

The Neumann boundary conditions can be used in conjunction with energy balance:

$$k\frac{\partial T}{\partial n} = h(T - T_0), \tag{6}$$

where h is the total heat transfer coefficient for the area near the simulated model boundary ($h = 430$ W/m^3·K), and T_0 is the ambient bulk temperature.[70] Studies show that the thermal conductivity of tissue changes with temperature.[71] The following equation is used for more accurate calculations:[72]

$$k(T) = k_0 + \Delta k[T - T_0], \tag{7}$$

where k_0 is the baseline thermal conductivity, Δk is the change in k due to temperature, and T_0 is the reference temperature at which k_0 is measured.

The nanoantenna transmits heat energy at a constant rate into the tumor tissue and liver. This radiation affects the tissue according to the absorption coefficient (α). The temperature (T) depth r from the point where the antenna is connected to the catheter, at time t after starting the heat flow is as follows:

$$T(r,t) = \frac{2H}{k}\sqrt{\psi t}\ \text{ierfc}\left[\frac{r}{2}\sqrt{\frac{kt}{\rho c}}\right], \tag{8}$$

where H is the heat transfer ratio, and the ierfc function is given by the following relation:

$$\text{ierfc}(u) = \frac{1}{\sqrt{\pi}}\left\{\exp(-u^2 - u(1 - (2\sqrt{\pi}) \times \int_0^u \exp(-t^2)\,\mathrm{d}t\right\}. \tag{9}$$

Since in this study, the catheter is located adjacent to the tissue, changes in tissue surface temperature with time can be obtained by placing $(r = 0)$ in Eq. (8) as follows:

$$\Delta T(0,t) = \left(\frac{2T}{k}\right)\left(\frac{kt}{\pi\rho c}\right)^{1/2}. \tag{10}$$

Note that $\text{ierf}(0) = 1/\sqrt{\pi}$. As a result, for preventing to increase indefinitely temperature and produce damage in the surface of the tissue, the heat must be supplied for a limited time (t_p) and then cut off. That is, a pulsed excitation source must be used for the nano-antenna.

The amount of tumor damage can be calculated by integral and using the Arrhenius equation as follows:[73]

$$\frac{\mathrm{d}\beta}{\mathrm{d}t} = f\exp\left(\frac{-\Delta E_a}{R_g T}\right), \tag{11}$$

$$\beta = \int_0^t f\exp\left[\frac{-E_a}{R_g T}\right]\mathrm{d}t, \tag{12}$$

where β determines the amount of damage to the tumor, f is the frequency coefficient, and E_a is the activation energy. These two parameters depend on the type of tissue. R_g is the gas constant, and T is the absolute temperature. This integral evaluates the energy accumulated in the tissue over time. In general, the β parameter is expressed through the fraction of tissue necrosis θ_d, which is defined as follows:[74]

$$\theta_d = 1 - \mathrm{e}^{\beta}. \tag{13}$$

The excitation power, radiation wavelength, pulse duration are important in hyperthermia. The nano-antenna resonance wavelength can be determined analytically using a simple Fabry–Pérot model, which analyzes the nano-antenna.[75,76] The Fabry–Pérot analytical model is used for studying geometrical effects and resonance wavelengths of the nano-antenna. In this model, the resonance wavelength λ_{res} reads

$$\frac{\lambda_{res}}{2n_{eff}} = L + 2\zeta, \tag{14}$$

where n_{eff} is the effective index of the surface charge wave, and ζ is due to the reactance of the nano-antenna ends.[75] Usually, ζ is of the order of the lateral dimension of the nano-antenna.[75,77]

Directivity is a fundamental nano-antenna parameter. It shows the amount of the concentration of a nano-antenna radiation pattern in a particular directio. Ideally, if a nano-antenna has high directivity, the interaction of the set of directed emission modes with the tissu will be enhanced. In the emitter nano-antenna, directivity evaluates as follows:

$$D(\theta,\varphi) = 4\pi\left[\frac{P_{ang}(\theta,\varphi)}{\iint P_r(\theta,\varphi)\,\mathrm{d}\Omega}\right], \tag{15}$$

where $P_{ang}(\theta,\varphi)$ is the angular power density, and $P_r(\theta,\varphi)$ is the angular radiated power of the scattered far-field in a given direction (θ and φ), and the integral is over all angles.[78]

3. Modeling and design of the nano-antennas

The studied nano-antennas in this study consist of the SEDNA [Fig. 1(a)] and the LSFNA [Fig. 1(b)]. The center of the SEDNA gap in both nano-antennas is placed in the coordinate origin and their arms are aligned along the x-axis and their thickness in the z-direction (Fig. 1). The SEDNA dimension parameters are defined as length L, width W, and thickness H. As shown in Fig. 1(b), four L-shaped nanomaterials make an L-shaped frame around the SEDNA. According to this figure, the gap between the LSF and the SEDNA is d. Note that adjusting the gap between the L-shaped frame (LSF) and the SEDNA is very important and large values of d will decrease the SEDNA and the LSF interactions. The LSFNA dimension

parameters are defined as length L_f, width W_f, and thickness H_f.

Note that the inner SEDNA of the LSFNA in Fig. 1(b) is the same as the SEDNA defined in Fig. 1(a) and the LSFNA dimensions L_f, W_f, and H_f are proportional to the SEDNA dimensions L, W, and H, and the air spacing d between the LSFNA and the SEDNA has been kept to be unchanged. All structures are made from gold in the air substrat.

As shown in Fig. 1, a sinusoidal voltage V_s applied to the gap(s) of the nano-antenna. According to Fig. 1(b), the LSF consists of four electric dipole nano-antennas with long and short lengths, which are placed in pairs in front of each other, the length of the long electric dipole nano-antenna is equal to L_f, and the length of the short dipole nano-antenna is equal to (W_f. As shown in Fig. 1(b), these nano-antennas are numbered from 1 to 4.

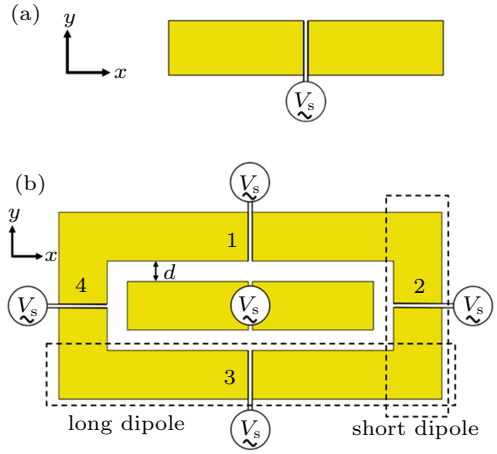


Fig. 1. Structures of (a) the SEDNA and (b) the LSFNA.

4. Results

4.1. The nano-antenna specifications

We investigated the effects of geometrical specifications of the nano-antenna on its radiation characteristics (such as the near- and far-field intensities, directivity, and sensitivity) using invasive thermal ablation of cancerous tumors by the FE. The target wavelength range for the study of the nano-antenna radiation characteristics is selected from 0.5 μm to 3 μm.

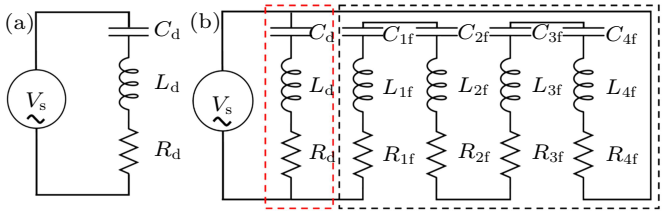


Fig. 2. Equivalent circuits of (a) the SEDNA and (b) the LSFNA.

Before starting the studies, it should be determined using the equivalent RLC circuit method to show the effect of using the LSF on the SEDN. The equivalent electrical RLC circuits[62] of the SEDNA and the LSFNA are shown in Fig. 2. According to Fig. 2(a), the sinusoidal voltage V_s is connected to both ends of the SEDNA equivalent circuits. According to Fig. 2(b), the equivalent circuit of the L-shaped frame (LSF) consists of four RLC amplifiers connected in series. Thus, the equivalent RLC circuit of the LSFNA is a parallel connection of the equivalent circuit of the SEDNA and the LSF. In comparison of Figs. 2(a) and 2(b), it can be seen that by utilizing the LSF around the SEDNA, four amplifiers are connected to the SEDNA. As a result, it is expected that, in addition to the enhancement of the radiation characteristics of the SEDNA, they become adjustable under the influence of the LSF. By ignoring any of the fringe effects on the RLC elements, we can calculate the impedance using the following equation:

$$Z = \mathrm{i}\frac{(L,\ \text{or},\ L_f)}{\omega\varepsilon\varepsilon_0}(W,\ \text{or},\ W_f)\times(H = H_f). \tag{16}$$

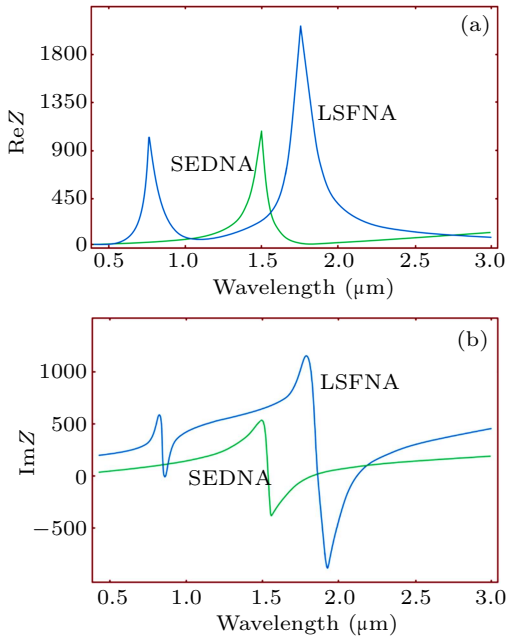


Fig. 3. (a) Real impedance (Z) and (b) imaginary impedance (Z) for the SEDNA and the LSFNA.

From Fig. 3, it can be seen that the SEDNA real and imaginary parts of impedance have not only red-shift but also an enhancement after using the LSF. Note that, in this figure, the SEDNA dimensions are $610 \times 120 \times 60$ nm and the LSFNA dimensions are $950 \times 460 \times 60$ nm.

4.2. Geometrical effects on the far-field and directivity

Using the nano-antennas in thermal ablation requires to consider the far-field radiation. To enhance the far-field radiation of a nano-antenna, its structures must be modified. Figure 4 shows the effects of the dimension variations of the SEDNA and the LSFNA on the far-field intensity and the far-field radiation pattern (FFRP) in angular distribution and 3D form respectively. Note that all color-bars of the 3D FFRPs in Fig. 4 are set at the same value. To study the far-field of

the SEDNA and the LSFNA, we assume that all of the gap widths in both nano-antennas are fixed at 10 nm, and calculations of the far-field intensities and FFRPs in our models are plotted for a detector located at 1 mm above the nano-antennas in z-direction. In Fig. 4, the far-field intensities are plotted in xz-plane.

Figure 4(a) shows the far-field intensity for the SEDNA when the length L changing from 410 nm to 1010 nm, and it has been maximized at 90° in xz-plane. Figure 4(b) shows the far-field intensity for the LSFNA for different length L_f from 750 nm to 1350 nm. Note that the LSF length L_f increasing proportionally with the inner SEDNA width L. This figure shows that the far-field intensity of the LSFNA has a maximum value in 90° in xz-plane. From Figs. 4(a) and 4(b) it is obvious that the far-field does not change significantly with increasing length in both nano-antennas, and using LSF around SEDNA will cause an enhancement in far-field intensity.

Figure 4(c) shows the far-field intensity of the SEDNA for different width W from 30 nm to 120 nm, and it can be seen that the far-field intensity is increased due to the increasing width. Also, the far-field intensity has been maximized at 90° in xz-plane. Figure 4(d) shows the far-field intensity for the LSFNA when the width W_f changing from 190 nm to 460 nm. Note that the LSF width W_f increasing proportionally with the inner SEDNA width W. It can be seen that the far-field intensity is not only increased by increasing the width but also enhanced due to using the LSF.

Figure 4(e) shows the far-field intensity of the SEDNA for changing the thickness H from 60 nm to 120 nm, and it is obvious that the far-field intensity is decreased due to increasing the thickness. Also, the far-field intensity has been maximized at 90° in xz-plane. Fig. 4(f) diagrams show the far-field intensity for the LSFNA when the thickness (H_f) changing from 60 nm to 120 nm. Note that the LSF thickness (H_f) is the same as the inner SEDNA thickness (H). The far-field intensity decreased by increasing thickness (H and H_f). As can be seen from Figs. 4(b), 4(d), and 4(f), the LSF enhanced the far-field intensity approximately about 3-times.

From Figs. 4(a), 4(c), and 4(e), it can be seen that the SEDNA's FFRP is donut-shaped and has a uniform spatial distribution in YZ-plane, and Figs. 4(b), 4(d), and 4(f) show the dumbbell-shaped spatial distribution of the LSFNA's FFRP and it is pulled along the Z-direction, i.e. the polarization direction of the LSFNA emitting is along the Z-axis. Considering FFRPs for different situations in Fig. 4, revealed that the SEDNA's donut-shaped FFRP has been deformed to a dumbbell-shaped FFRP by using the LSF. This is useful for some applications which need to control the spatial distribution of radiation. Note that, for the SEDNA, the far-field radiation increases slowly with the antenna dimension variations. Also, adding the LSF around the SEDNA causes more sensitivity of intensity to dimension variations.

According to Fig. 5, directivity (D) is plotted based on wavelength and angular distribution, which shows the propagation direction of the nano-antennas. This figure presents wavelength-dependent directivity (D) for different lengths (L and L_f), but W_f, and $H = H_f$ are kept fixed at 460 nm and 60 nm respectively. In Fig. 5(a), the directivity has been red-shifted and increased when length (L) increased in the SEDNA. From Fig. 5(b), it is obvious that the directivity (D) increased about 1.4-times by using the LSF. Also, the directivity (D) is red-shifted and decreased with increasing length (L_f) for the LSFNA. Furthermore, the angular distribution of directivity (D) for two mentioned nano-antenna lengths are plotted, which shows that the directivity (D) of the LSFNA (Fig. 5(b)) is more localized in space than the SEDNA (Fig. 5(a)).

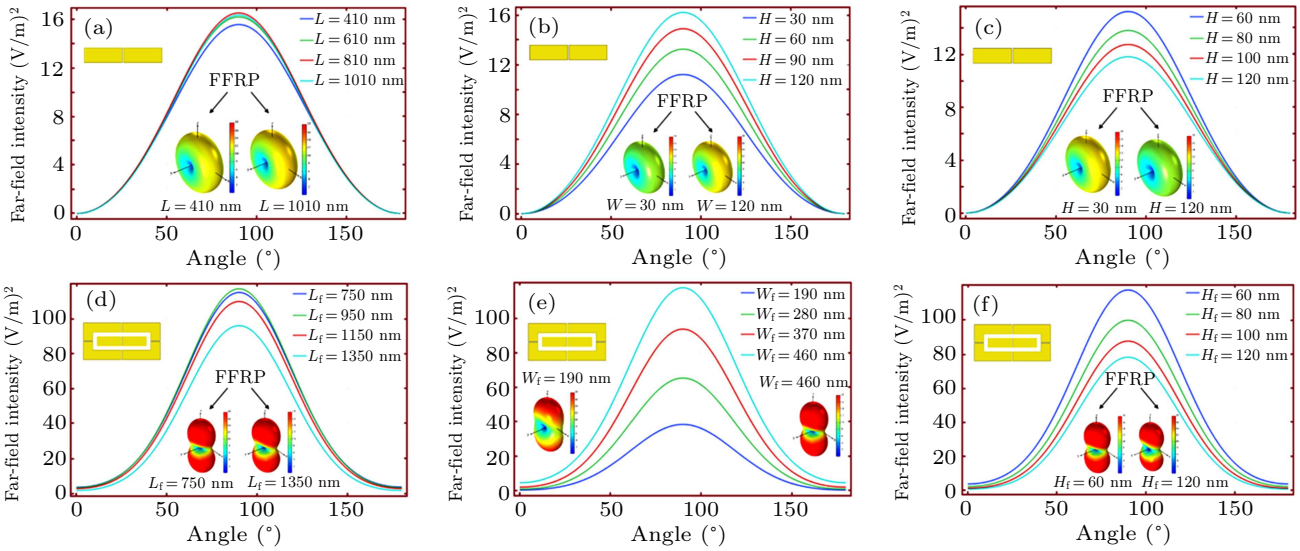


Fig. 4. The far-field intensity and the FFRP of the SEDNA with different (a) length (L), (c) width (W), and (e) thickness (H), and the far-field intensity and the FFRP of the LSFNA whit different (b) length (L_f), (d) width (W_f), and (f) thickness (H_f).

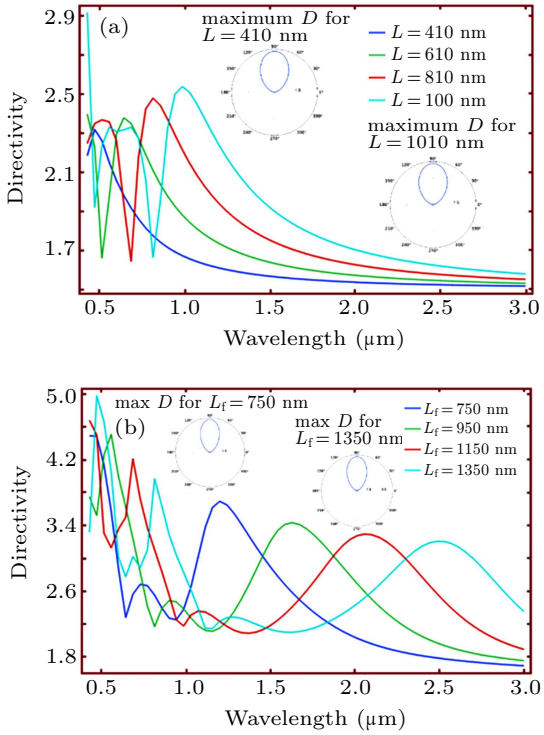


Fig. 5. Directivity for (a) the SEDNA, and (b) the LSFNAs. The angular distributions of directivity are plotted for two mentioned nano-antenna lengths in *xz*-plane.

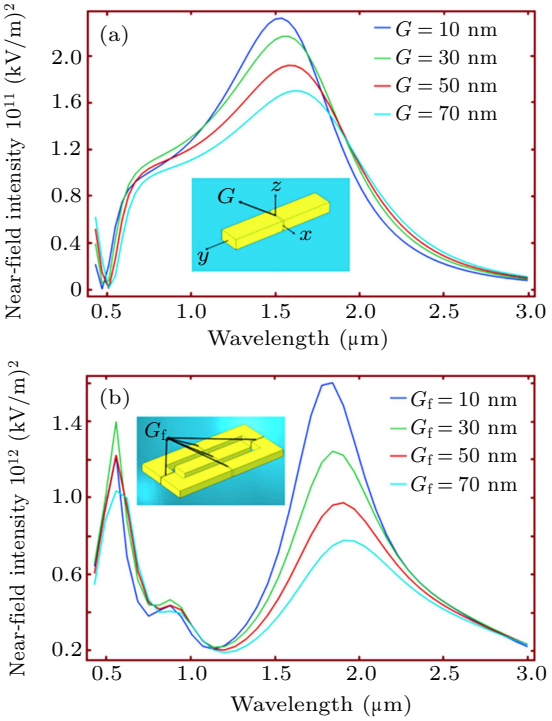


Fig. 6. Near-field intensity variations in (a) the SEDNA and (b) the LSFNA due to different gap widths G and G_f.

The results in Fig. 5 show that the directivity (D) of the SEDNA became the same for a higher wavelength and converge (i.e. D intends to 1.5). Also, using the LSF caused an increase in the resolution of the directivity (D) in Fig. 5(b) in comparison to the SEDNA directivity (D) in Fig. 5(a).

From Fig. 5, it can be seen that the LSFNA can achieve higher directivity. Use the LSF around the SEDNA caused an increasing directivity D and transforms the SEDNA from omnidirectional to the one-directional emitter. It is worth nothing to say that the LSF acts as shield around the SEDNA, and confine the SEDNA's radiated energy in z-direction. Thus, according to energy conservation, the LSFNA's FFRP becomes dumbbell-shape and its directivity is enhanced. Thus, the LSFNA is an ideal candidate for the thermal ablation of cancer cells in the tissue.

4.3. Gap width effects on the near-field intensity and the sensitivity

In this section, the gap widths ($G = G_f$) effect of the nano-antennas is investigated on near-field intensity and sensitivity. Figure 6 shows the near-field intensity of two nano-antenna structures with $L = 610$ nm for the SEDNA, and $L_f = 950$ nm for the LSFNA. Here W and H are kept to be fixed at 120 nm and 60 nm, respectively, for SEDNA, and W_f and H_f are kept to be fixed at 460 nm and 60 nm for the LSFNA.

Figure 6(a) shows that increasing G leads to a red-shift in near-field intensity and a linear reduction of it. According to Fig. 6(b), it is obvious that the near-field intensity of the LSFNA decreases and it red shifts with increasing the longitudinal distance of G_f.

The results show that there is a stronger dependence of the near-field intensity of the LSFNA with its gap width variation than the SEDNA. As shown in Fig. 6, increasing the gap width can decrease the near-field intensity, and comparing Figs. 6(a) and 6(b) gives that the near-field intensity using the LSFNA decreases faster.

It can be seen that with decreasing gap widths, the nano-antenna resonances show red-shift as the same as the experimental results for nano-discs described by in Ref. [79]. The sign of the interaction field between the two arms can alternate as a function of the gap between them.[78,80] For short enough distances, the near-field interaction dominates, and the gap between the arms acts as a nano-inductor with opposite charges on facing antenna ends.[81] Large near-field enhancements[82,83] are of strong interest for many applications. As shown in Fig. 6, one way to obtain high intensity enhancements in the near-field is to reduce the distance between nano-arms to increase coupling fields. For the case of nearly touching arms, one expects huge near-field enhancements.[76]

The sensitivity of the SEDNA and the LSFNA resonances is plotted versus the gap width variations in Fig. 7. The sensitivity to gap width is defined as intensity to gap width at the resonance wavelength. Furthermore, the near-field intensity of nano-antennas is very sensitive to their gap width (G and G_f) variations, so when the gap width increases as shown in Fig. 7, a linear attenuation happens on their sensitivity. Comparing orange and blue lines in Fig. 7 illustrates that the LSFNA is more sensitive to the gap width variations. In this study, the sensitivity in the SEDNA decreases 1.2 times by increasing the gap width from 10 nm to 70 nm, and the LSFNA decreases

2.3 times. Thus, more sensitivity can be achieved by decreasing the gap width. We can use this information as a design rule to tune nano-antenna for different applications.

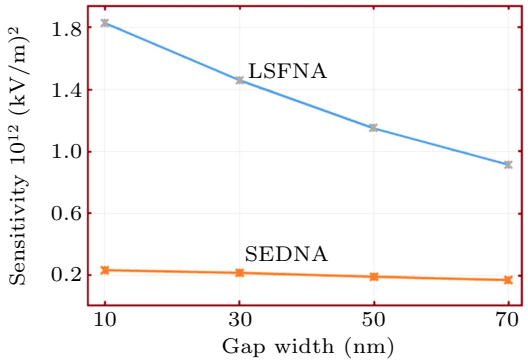


Fig. 7. The near-field sensitivity to gap width variations in (a) the SEDNA and (b) the LSFNA.

4.4. Thermal ablation

Thermal ablation therapy for cancerous tumors involves using heat to kill cancer cells in a tumor. Therefore, the cancer cells inside the tumor are irradiated by using an array of LSFNA that are placed on a parabolic dielectric substrate as shown in Fig. 8. The antenna is placed next to the tumor by a catheter and focuses the energy at its center. This energy is converted into heat and causes damage to biological tissues.

4.4.1. Modeling and design of the liver and the inserted antenna

The antenna (LSFNA array) is connected to a pulsed electrical source by a transmission line with a radius of 1.3 mm covered by a dielectric with a thickness of 0.5 mm. Note that the voltage source (generator) has a tunable excitation input power. The antenna operates at its resonance wavelength. The dimensions of the nano-antenna are shown in Fig. 8. An arbitrary cancerous tumor with a length of 10 mm has been considered.

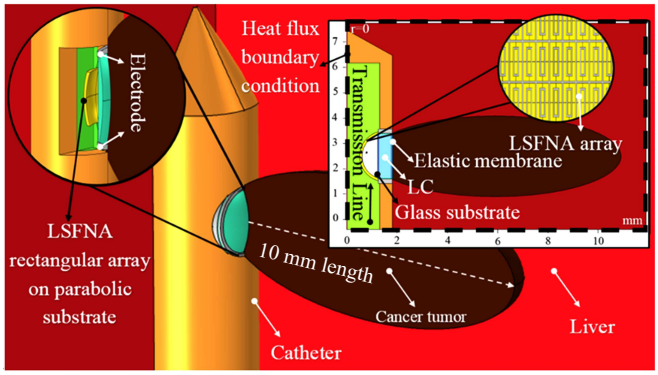


Fig. 8. Simplified scheme of optical nano-antenna in liver tissue and adjacent to cancerous tumor in dimensions 2 and 3.

The heat flux within the surrounding walls of the liver is equal to zero ($\hat{n}\,(k\nabla T) = 0$), where $\hat{n}$ is the unit vector normal to the boundaries of the calculation region (dashed line in Fig. 8). The heat flux is continuous within the interface between the tumor and the liver, ($k_{\text{tumor}}\,(T)\,\nabla T_{\text{tumor}}\,(T) = k_{\text{liver}}\,(T)\,\nabla T_{\text{liver}}\,(T)$). As shown in Fig. 8, the LSFNA with $L_{\text{f}} = 950$ nm is designed in an array form on a parabolic substrate, and positioned in front of a tunable liquid crystal lens. The LC lens is designed in such a way that consists of a polarizer, a glass substrate, an LC layer, an elastic membrane. Also, both the glass substrate and the elastic membrane are coated with transparent electrodes and alignment layers. Furthermore, the alignment layers are mechanically buffered in anti-parallel directions. The polarizer is used to filter out the ordinary wave of the incident light. This lens is used to increase the accuracy of the antenna and adjust the focus of its radiation field along the tumor region. The total focal length of the LC lens can be written as[84–86]

$$f(V) = \frac{f_{\text{e}} R}{f_{\text{e}}(n_{\text{eff}}(V) - 1) + R}, \tag{17}$$

where R is the radius of the elastic membrane curvature, $n_{\text{eff}}(V)$ is a voltage-dependent effective refractive index of the LC layer, f_{e} is the focal length of the elastic membrane. As seen in Fig. 9, the focal length of this lens is changed by utilizing an electric field in the electrodes. This electrically variable focus lens is working as a process based on Refs. [87,88].

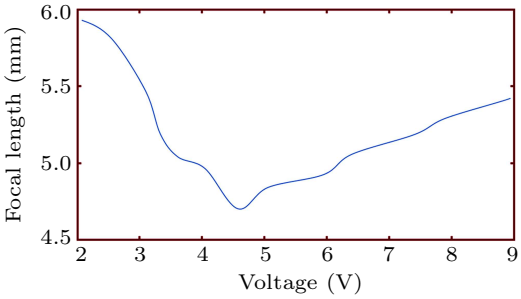


Fig. 9. The relationship between the focal length of the LC lens and the applied signal voltage.

4.4.2. The penetration depth of the electric field

One of the most important parameters in the thermal ablation process is the penetration depth of the electric field in the cancerous tumor. Figure 10 shows the propagation of the electric field in the liver tissue. According to this figure, the electric field penetrates the liver tissue up to 20 mm approximately. According to the antenna structure, the maximum electric field

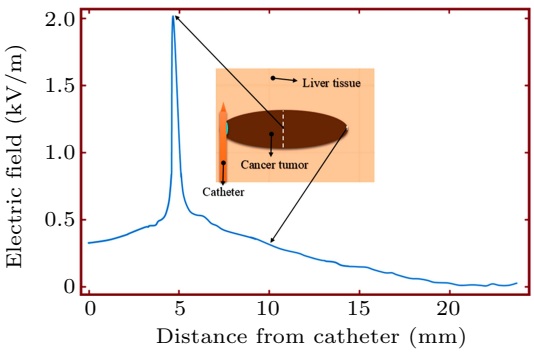


Fig. 10. Propagation of the electric field in the liver tissue.

is obtained at a distance of 5 mm from the catheter, which not only reduces the possibility of damage to the antenna at high temperatures but also causes more energy to be concentrated within the cancerous tumor. Also, concentrating all of the energy on the cancerous tumor region reduces the risk of damage to healthy tissues.

4.4.3. Special absorption rate

During the irradiation process, the electromagnetic wave is propagating through the nano-antenna into the biological tissue and the energy of this wave is absorbed through the materials. Therefore, another important parameter is the special absorption rate (SAR), which indicates the absorbed power density normalized by tissue density. To estimate the ability of heating tissue, in Fig. 11, according to Eq. (4), the SAR diagram is drawn for different excitation input powers of the voltage source in 10 s of heating at a distance of 5 mm from the catheter axis in front of the antenna. Note that these input powers belong to the generator that provides the sinusoidal voltage to excite the antenna.

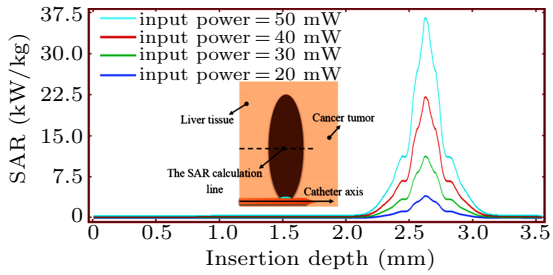


Fig. 11. Axial profile of SAR after 10 s for different excitation input powers.

According to Fig. 11, it can be seen that the SAR diagram increases with the excitation input power increasing. Also, the SAR is increased perpendicular to the axis parallel to the length of the catheter, and the peaks of its graphs are on the z-axis. As is expected, the designed antenna concentrates the peaks of SAR in the tumor area and it is also observed that the SAR diagrams in the healthy regions of tissue tend to zero.

Chen *et al.*[9] studied the photo-thermal therapy of the cancer cells by gold nanorods. They showed that using the cluster form of the gold nanorods in the cancer cells lysosomes causes increase in the absorption and two-photon luminescence of the gold nanorods. The results reported in this study show that due to plasmonic coupling between gold nanorods, using an array of the gold nanorods in a cluster form compared to using them separately (isolated) will increase the absorption rate and thus improve the treatment process.[9] According to the reciprocal lattice theory,[43] a nanoantenna can not only act as a receiver and generate a local field but also act as a transmitter with far-field characteristics. In one sense, an LSFNA array is a cluster of gold nanorods arranged in one direction that enters into the cancer cells through a catheter. As a result, according to Fig. 11, it can be seen that the specific absorption rate of the proposed antenna has increased with the increasing excitation power of the LSFNA. The antenna designed in this research is similar to the antenna designed by Jiang *et al.* in the field of microwave thermal ablation.[51,53,57] Using the microwave antenna in cancer treatment of small tumors is associated with a high risk of damage to healthy cells. Thus, it is suggested that the proposed antenna in Fig. 8 is suitable for small tumors. Comparing the results obtained in Fig. 11 with the results reported in Ref. [53] clears that the proposed antenna has a sufficient specific absorption rate in the tumor tissue.

4.4.4. Temperature distribution

The main feature related to the function of this antenna for the cancerous tumors ablation is the temperature. Therefore, the system should be designed in such a way that tumor ablation as a heat treatment method, without damaging healthy tissue, eliminates cancerous tumors. Consequently, a study on temperature effects and temperature control is required.

Figure 12 shows the temperature distribution (Eq. (8)) in terms of distance from the catheter in the biological tissue, which is plotted for different excitation input powers. As can be seen, a probe line passes through the cancerous tumor from left to right, and the temperature has been evaluated on this line at each point of distance r from the catheter. Note that the graphs show the similar behavior with increasing temperature. The temperature has increased to the maximum amount at 5 mm away from the nano-antenna. After that, the temperature drops significantly with increasing distance. As a result, the maximum amount of temperature is created in the tumor region. Note that the temperature rises rapidly as the excitation input power increases. Therefore, if this temperature increase is more than normal, it also destroys healthy cells.

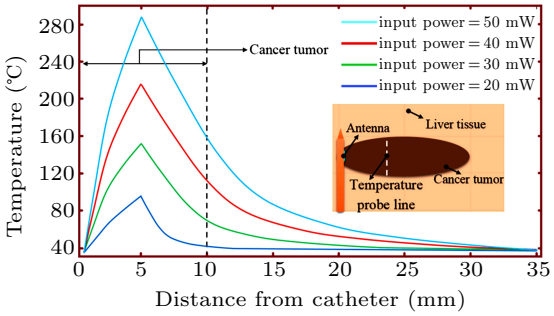


Fig. 12. Temperature distribution in liver and tumor tissue versus the function of location in the 10 s of heating for different excitation input powers.

In this structure, the electrical field is well enhanced by utilizing the LSFNA and radiated to the tumor with high directivity. In this optical system, a modulated electric field is applied to the LC lens by the cathode, which causes a reorientation of LCs. Then, the lens focus has changed and the antenna can radiate more accurately. In addition, the use of pulsed excitation input power increases the radiation control of the antenna. As shown above, the LSFNA has high directivity. As a result, the risk of damage to healthy tissue is greatly

reduced. However, it is important to note that the temperature increases with the excitation input power, which increases the possibility of damage to the healthy tissues. According to Fig. 12, with the excitation input power of $P = 20$ mW the tumor region is well irradiated and the healthy tissues are safe.

Hence, there is a very low risk of damage to healthy tissues when choosing a suitable excitation input power and a well-adjusted optical system. Therefore, the central part of the tumor kills, but its outer layer, may not heal completely. Therefore, the input power must increase slightly to ensure that the whole tumor region is irradiated. However, by doing this action, the risk of damage to healthy tissues around the tumor threatens this process. According to Fig. 12, it seems that using an excitation input power of about 20 mW is sufficient to treat a tumor with a radius of about 10 mm. The required time duration of this process is discussed in the next section. Note that, if it is necessary to use higher excitation input powers, a very short heating time should be chosen. This may reduce the possibility of damage to healthy tissues. Therefore, by extending these results, the optimal excitation input power for a tumor can be found.

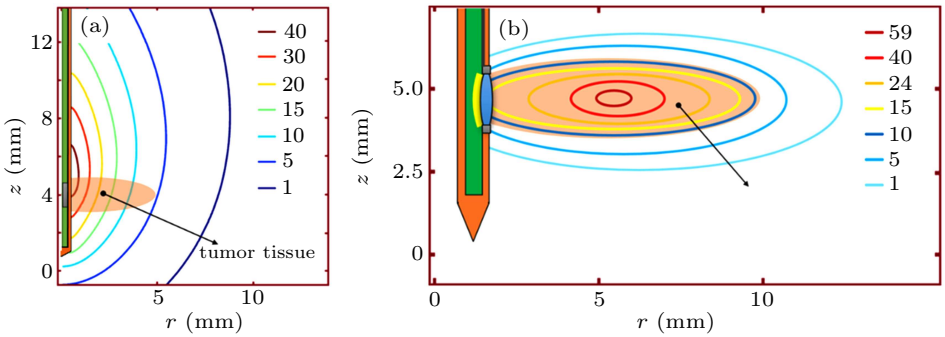


Fig. 13. Spatial temperature distribution within biological tissue for (a) the microwave antenna[53] and (b) the proposed antenna.

Figure 13 shows the temperature distribution diagram of electromagnetic radiation in the liver tissue for two microwave antennas (Fig. 13(a)) in 300 s and $P = 10$ W, and the proposed antenna (Fig. 13(b)) in 1.6 s and $P = 20$ mW. It is worth noting that Fig. 13(a) is drawn using the information reported in Ref. [53]. According to Fig. 13(a), it can be seen that using the microwave antenna in a small tumor damages the healthy tissue. In contrast, the results obtained in Fig. 13(b) show that the proposed antenna entirely radiates the tumor area and prevents damage to the adjacent healthy cells.

Therefore, the results obtained in Figs. 12 and 13 show that the temperature distribution can be controlled more favorably in small tumors using the proposed antenna than microwave antennas.

4.4.5. The fraction of tissue necrosis

Figure 14 shows the changes in the tumor damage during ablation at different distances from the catheter in the liver tissue (Eq. (13)). This figure is drawn for different excitation input powers. According to Fig. 14, it can be seen that

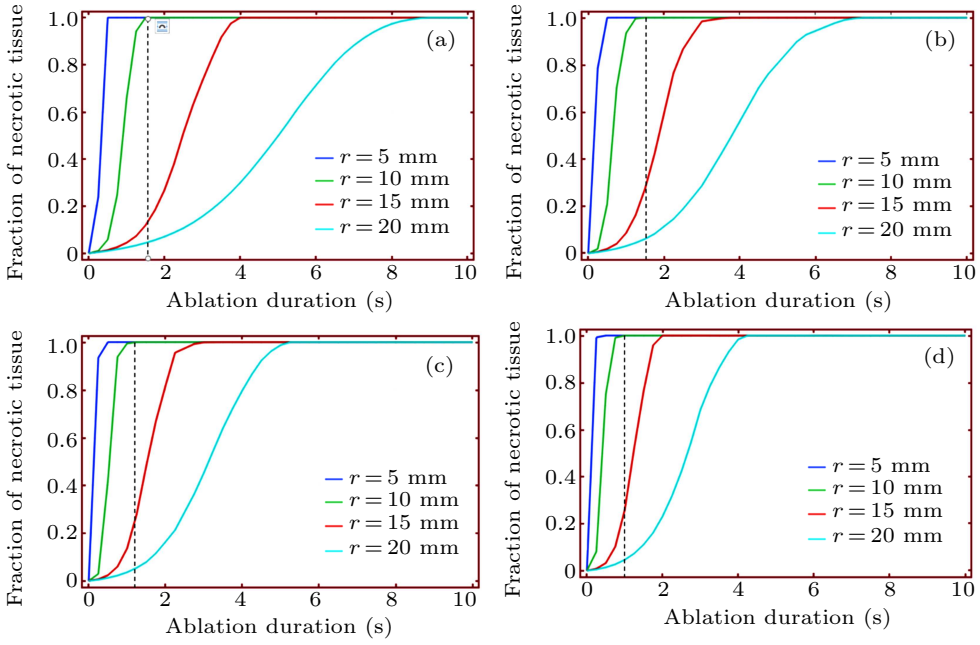


Fig. 14. Comparison of the fraction of necrotic tissue for four positions from the catheter, during the ablation duration time for different excitation input powers as (a) $P = 20$ mW, (b) $P = 30$ mW, (c) $P = 40$ mW, and (d) $P = 50$ mW.

the change in the damaged tumor gradually increases and then reaches the saturation zone, which indicates the time of completion of tumor necrosis. According to the numerical results, the time required for complete necrosis in the tumor is equal to 1.6 s, 1.45 s, 1.25 s, and 1 s (shown by black dashed lines) for the excitation input powers of 20 mW, 30 mW, 40 mW, and 50 mW respectively. Therefore, when the antenna excitation input power is very high, the time required for complete tumor ablation is very short. However, in the case of a lack of care, the risk of damage to healthy tissues will increase. If the low excitation input power is used, it is possible to destroy the tumor for a long time without damaging healthy tissues.

5. Conclusions

In summary, using the results obtained by the proposed antenna, the cancer treatment in the liver tissue based on thermal ablation is analyzed. To investigate the thermal ablation of tumors in biological tissue, the appropriate thermodynamic and optical characteristics of the biological tissue (such as density, thermal conductivity, specific heat capacity, and electrical conductivity) must be used. Also, the vascular, neurological, or bony nature of the tumor tissue must be considered in the electromagnetic and bio-heat calculations. Hence, the heat transfer associated with the propagation of electromagnetic waves radiated from the L-shaped frame nano-antenna (LSFNA) in liver tissue for different excitation input powers is investigated. For this purpose, the antenna design and optimization process are performed in two steps. First, the LSFNA is designed and used as a source for liver tumor ablation. Thus, the effect of using the LSF around the SEDNA is analyzed by the equivalent RLC circuit method. Then, the radiation characteristics of this nano-antenna are studied and compared with SEDNA using FEM simulations. Using the LSF around the SEDNA enhances and modifies the radiation characteristics of this nano-antenna, such as far-field intensity and directivity. Also, the sensitivity of the SEDNA to the gap width increases after using the LSF. Furthermore, the FFRP of the SEDNA shifts from a donut-shaped form with a 2.5-times increase to a teared-shaped pattern. The LSFNA confined the electric field inside the LSF, as a result, the directivity increases by more than 1.5 times in this nano-antenna, and resulting in a higher resonance wavelength shift rate and thus higher resolution than the SEDNA. Hence, the LSFNA is designed and optimized in this manner. Another feature of the LSFNA is its adjustability in the nano-antenna performance proportional to the LSF dimensions. Therefore, the SEDNA radiation characteristics can be resonating at higher or lower wavelengths without the need to change in its geometry dimensions, which helps us to design different nanostructures for biomedical applications such as spectroscopy for defining different materials. As a result, the spectral characteristics (resonance wavelength), wavelength shifts, near-field and far-field intensities, resolution, and directivity of a nano-antenna can be adjusted.

In the next step of this investigation, an antenna is designed to use in the thermal ablation process. Thus, the liver and cancerous tumor tissues are simulated and the designed antenna is inserted into them. In this antenna, the LSFNA which is excited with a pulsed sinusoidal voltage is studied to cancer treatment applications. The short-pulsed source is used to form a controlled heat generation by the nano-antenna to prevent damage to the healthy tissue cells. Furthermore, an LC tunable lens is used to increase the accuracy of the antenna to radiate the energy into the tumor cells. The temperature distribution profile, the specific absorption rate (SAR), and the fraction of necrotic tissue within cancer cells are obtained. The results show that SAR and temperature distribution are strongly affected by the antenna excitation input power. The SAR and the temperature appear to be very high in the center of the cancerous tumor due to utilizing a tunable LC lens and then decreased by moving away from this point. The maxima of the SAR and temperature are reached inside the tumor region. Finally, the suitable temperature and the optimum excitation input power of the antenna, and the thermal-ablation duration time are obtained by the simulations.

Although in this research we have used the proposed antenna in liver cancer treatment, it can be used in cancer treatment of the other biological tissues such as kidney, lung, and breast.

References

[1] Goldberg S N, Grassi C J, Cardella J F, Charboneau J W, Dodd III G D, Dupuy D E, Gervais D A, Gillams A R, Kane R A and Lee Jr F T 2009 *J. Vasc. Interv. Radiol.* **20** S377

[2] Jalali R, Munshi A and Arora B 2009 *Neurol. India* **57** 13

[3] Triesscheijn M, Baas P, Schellens J H M and Stewart F A 2006 *Oncologist* **11** 1034

[4] Durante M and Loeffler J S 2010 *Nat. Rev. Clin. Oncol.* **7** 37

[5] Kennedy J E 2005 *Nat. Rev. Cancer* **5** 321

[6] Conde J, Bao C, Cui D, Baptista P V and Tian F 2014 *J. Control. Release* **183** 87

[7] Abadeer N S and Murphy C J 2016 *J. Phys. Chem. C* **120** 4691

[8] Abbas M, Kessentini A, Loukil H, Muneer P, Ijyas V P T, Bushara S E and Wase M A 2019 *Nanoscale Res. Lett.* **14** 289

[9] O'Neal D P, Hirsch L R, Halas N J, Payne J D and West J L 2004 *Cancer Lett.* **209** 171

[10] Anger P, Bharadwaj P and Novotny L 2006 *Phys. Rev. Lett.* **96** 113002

[11] Bharadwaj P, Deutsch B and Novotny L 2009 *Adv. Opt. Photon.* **1** 438

[12] Liu Z K, Xie Y N, Geng L, Pan D K and Song P 2016 *Chin. Phys. Lett.* **33** 27802

[13] Li T-J, Liang J-G, Li H-P and Liu Y-Q 2016 *Chin. Phys. B* **25** 94101

[14] Li X, Sun J D, Huang H J, Zhang Z P, Jin L, Sun Y F, Popov V V and Qin H 2019 *Chin. Phys. B* **28** 118502

[15] Zhou T Y 2019 *Acta Phys. Sin.* **68** 055201 (in Chinese)

[16] Grober R D, Schoelkopf R J and Prober D E 1997 *Appl. Phys. Lett.* **70** 1354

[17] Crozier K B, Sundaramurthy A, Kino G S and Quate C F 2003 *J. Appl. Phys.* **94** 4632

[18] Muehlschlegel P, Eisler H-J, Martin O J F, Hecht B and Pohl D W 2005 *Science* **308** 1607

[19] Schuck P J, Fromm D P, Sundaramurthy A, Kino G S and Moerner W E 2005 *Phys. Rev. Lett.* **94** 17402
[20] Taminiau T H, Stefani F D, Segerink F B and Van Hulst N F 2008 *Nat. Photon.* **2** 234
[21] Wiley B J, Qin D and Xia Y 2010 *ACS Nano* **4** 3554
[22] Linden S, Kuhl J and Giessen H 2001 *Phys. Rev. Lett.* **86** 4688
[23] Castillo R C 2013 *Functional Nanostructures Fabricated by Focused Electron/Ion Beam Induced Deposition* (Berlin: Springer Science & Business Media)
[24] Vesseur E J R, De Waele R, Lezec H J, Atwater H A, García de Abajo F J and Polman A 2008 *Appl. Phys. Lett.* **92** 83110
[25] Henzie J, Lee J, Lee M H, Hasan W and Odom T W 2009 *Annu. Rev. Phys. Chem.* **60**
[26] Xia Y and Whitesides G M 1998 *Annu. Rev. Mater. Sci.* **28** 153
[27] Bender M, Plachetka U, Ran J, Fuchs A, Vratzov B, Kurz H, Glinsner T and Lindner F 2004 *J. Vac. Sci. Technol. B Microelectron. Nanom. Struct. Process. Meas. Phenom.* **22** 3229
[28] Lee M H, Huntington M D, Zhou W, Yang J C and Odom T W 2011 *Nano Lett.* **11** 311
[29] Odom T W, Thalladi V R, Love J C and Whitesides G M 2002 *J. Am. Chem. Soc.* **124** 12112
[30] Henzie J, Barton J E, Stender C L and Odom T W 2006 *Acc. Chem. Res.* **39** 249
[31] Webb J A, Ou Y C, Faley S, Paul E P, Hittinger J P, Cutright C C, Lin E C, Bellan L M and Bardhan R 2017 *ACS Omega* **2** 3583
[32] Ou Y C, Webb J A, Faley S, Shae D, Talbert E M, Lin S, Cutright C C, Wilson J T, Bellan L M and Bardhan R 2016 *ACS Omega* **1** 234
[33] DasGupta D, von Maltzahn G, Ghosh S, Bhatia S N, Das S K and Chakraborty S 2009 *Appl. Phys. Lett.* **95** 233701
[34] Nie S and Emory S R 1997 *Science* **275** 1102
[35] Kneipp K, Kneipp H, Itzkan I, Dasari R R and Feld M S 1999 *Chem. Rev.* **99** 2957
[36] Kneipp K, Wang Y, Kneipp H, Perelman L T, Itzkan I, Dasari R R and Feld M S 1997 *Phys. Rev. Lett.* **78** 1667
[37] Kühner L, Semenyshyn R, Hentschel M, Neubrech F, Tarín C and Giessen H 2019 *ACS Sensors* **4** 1973
[38] Kim K, Yajima J, Oh Y, Lee W, Oowada S, Nishizaka T and Kim D 2012 *Small* **8** 892
[39] Thammawongsa N, Mitatha S and Yupapin P P 2013 *Artif. Cells, Nanomedicine, Biotechnol.* **41** 21
[40] Habash R W Y, Bansal R, Krewski D and Alhafid H T 2006 *Crit. Rev. Biomed. Eng.* **34**
[41] Lin J C, Hirai S, Chiang C L, Hsu W L, Su J L and Wang Y J 2000 *IEEE Trans. Microw. Theory Technol.* **48** 2191
[42] Ierardi A M, Floridi C, Fontana F, Chini C, Giorlando F, Piacentino F, Brunese L, Pinotti G, Bacuzzi A and Carrafiello G 2013 *Radiol. Med.* **118** 949
[43] Wang K, Tavakkoli F, Wang S and Vafai K 2015 *J. Biomech.* **48** 930
[44] Kundu B 2016 *Appl. Math. Comput.* **285** 204
[45] Talaee M R and Kabiri A L I 2017 *J. Mech. Med. Biol.* **17** 1750072
[46] Lin S M and Li C Y 2017 *J. Mech. Med. Biol.* **17** 1750029
[47] Deshazer G, Prakash P, Merck D and Haemmerich D 2017 *Int. J. Hyperth.* **33** 74
[48] Paul A K, Bandaru N K, Narasimhan A and Das S K 2014 *International Heat Transfer Conference Digital Library* (New York: Begel House Inc.)
[49] Dickerson E B, Dreaden E C, Huang X, El-Sayed I H, Chu H, Pushpanketh S, McDonald J F and El-Sayed M A 2008 *Cancer Lett.* **269** 57
[50] Hirsch L R, Stafford R J, Bankson J A, Sershen S R, Rivera B, Price R E, Hazle J D, Halas N J and West J L 2003 *Proc. Natl. Acad. Sci. USA* **100** 13549
[51] Jiang Y, Zhao J, Li W, Yang Y, Liu J and Qian Z 2017 *Med. Biol. Eng. Comput.* **55** 2027
[52] Curto S, Taj-Eldin M, Fairchild D and Prakash P 2015 *Med. Phys.* **42** 6152
[53] Selmi M, Bin Dukhyil A A and Belmabrouk H 2020 *Appl. Sci.* **10** 211
[54] Rattanadecho P and Keangin P 2013 *Int. J. Heat Mass Transf.* **58** 457
[55] Kuang M, Lu M D, Xie X Y, Xu H X, Mo L Q, Liu G J, Xu Z F, Zheng Y L and Liang J Y 2007 *Radiology* **242** 914
[56] Prakash P, Salgaonkar V A, Clif Burdette E and Diederich C J 2012 *Med. Phys.* **39** 7338
[57] Lubner M G, Brace C L, Hinshaw J L and Lee Jr F T 2010 *J. Vasc. Interv. Radiol.* **21** S192
[58] Von Maltzahn G, Park J H, Agrawal A, Bandaru N K, Das S K, Sailor M J and Bhatia S N 2009 *Cancer Res.* **69** 3892
[59] Zhao W and Karp J M 2009 *Nat. Mater.* **8** 453
[60] Abbas A, El-Said M and Mahmoud S F 2013 *PIERS Proceedings*
[61] Prodan E, Radloff C, Halas N J and Nordlander P 2003 *Science* **302** 419
[62] Yao Y, Kats M A, Genevet P, Yu N, Song Y, Kong J and Capasso F 2013 *Nano Lett.* **13** 1257
[63] Agio M and Alù A 2013 *Optical Antennas* (Cambridge: Cambridge University Press)
[64] Simanovskii D M, Mackanos M A, Irani A R, O'Connell-Rodwell C E, Contag C H, Schwettman H A and Palanker D V 2006 *Phys. Rev. E* **74** 11915
[65] Moritz A R and Henriques Jr F C 1947 *Am. J. Pathol.* **23** 695
[66] Tehrani M H H, Soltani M, Kashkooli F M and Raahemifar K 2020 *PLoS One* **15** e0233219
[67] Trujillo M and Berjano E 2013 *Int. J. Hyperth.* **29** 590
[68] Cavagnaro M, Amabile C, Bernardi P, Pisa S and Tosoratti N 2010 *IEEE Trans. Biomed. Eng.* **58** 949
[69] Shi J, Chen Z and Shi M 2009 *Appl. Therm. Eng.* **29** 1792
[70] Cho J, Yoon J, Cho S, Kwon K, Lim S, Kim D, Lee E S, Kim C H, Choi J W and Cheon C 2006 *Int. J. cancer* **119** 593
[71] Keangin P, Rattanadecho P and Wessapan T 2011 *Int. Commun. Heat Mass Transf.* **38** 757
[72] Wu X, Liu B and Xu B 2016 *Appl. Therm. Eng.* **107** 501
[73] Singh S and Repaka R 2017 *Appl. Therm. Eng.* **125** 443
[74] Jasiński M 2013 *Mol. Cell. Biomech.* **10** 183
[75] Novotny L 2007 *Phys. Rev. Lett.* **98** 266802
[76] Aizpurua J, Bryant G W, Richter L J, De Abajo F J G, Kelley B K and Mallouk T 2005 *Phys. Rev. B* **71** 235420
[77] Cubukcu E and Capasso F 2009 *Appl. Phys. Lett.* **95** 201101
[78] Dahmen C, Schmidt B and von Plessen G 2007 *Nano Lett.* **7** 318
[79] Massa E, Maier S A and Giannini V 2013 *New J. Phys.* **15** 63013
[80] Romero I, Aizpurua J, Bryant G W and De Abajo F J G 2006 *Opt. Express* **14** 9988
[81] Sundaramurthy A, Crozier K B, Kino G S, Fromm D P, Schuck P J and Moerner W E 2005 *Phys. Rev. B* **72** 165409
[82] Beversluis M R, Bouhelier A and Novotny L 2003 *Phys. Rev. B* **68** 115433
[83] Bouhelier A, Beversluis M, Hartschuh A and Novotny L 2003 *Phys. Rev. Lett.* **90** 13903
[84] BEA S and Teich M C 1991 *Wiley* 313
[85] Ji H S, Kim J H and Kumar S 2003 *Opt. Lett.* **28** 1147
[86] Sato S 1979 *Jpn. J. Appl. Phys.* **18** 1679
[87] Algorri J F, Zografopoulos D C, Urruchi V and Sánchez-Pena J M 2019 *Crystals* **9** 272
[88] Zohrabi M, Cormack R H and Gopinath J T 2016 *Opt. Express* **24** 23798